IEEE Access
Multidisciplinary | Rapid Review | Open Access Journal

Received March 29, 2019, accepted April 8, 2019, date of publication April 22, 2019, date of current version May 23, 2019.

Digital Object Identifier 10.1109/ACCESS.2019.2912305

Near Field Synthesis Based on Multi-Port Antenna Radiation Matrix Eigenfields

RENATO CICCHETTI[1], (Senior Member, IEEE), ANTONIO FARAONE[2], (Senior Member, IEEE), AND ORLANDINO TESTA[1]

[1]Department of Information Engineering, Electronics and Telecommunications, Sapienza University of Rome, 00184 Rome, Italy
[2]Devices Business, Motorola Solutions, Inc., Fort Lauderdale, FL 33322, USA

Corresponding author: Renato Cicchetti (renato.cicchetti@uniroma1.it)

This work was supported by the Italian Ministry of Education, University and Research, under Grant 20152HWRSL.

ABSTRACT The attainable performances of a general formulation employing radiation matrix eigenfields of multi-port antennas to synthesize near-field distributions are investigated. Field synthesis performed on open or closed surfaces, proximate to or enclosing an antenna array, either based on both electric and magnetic target field distributions or just the former, are presented to illustrate the key features of the synthesis technique and its sensitivity with respect to realistic random magnitude and phase variations of the array excitation profiles. Guidelines to perform synthesis and the steering of the complex near-field distributions are then suggested. The propagation characteristics of diffraction-resistant Bessel, OAM Bessel, and Airy beams in their actual finite-energy implementation, when they are excited by finite-size antenna arrays are finally investigated.

INDEX TERMS Airy beams, beam forming, Bessel beams, orbital-angular-momentum (OAM) beams, eigenmodes, eigenfields, multi-port antennas, near-field synthesis, radiation matrix, through-the-wall imaging, wireless power transfer (WPT).

I. INTRODUCTION

The design of modern microwave-sensing devices, high-resolution hyperthermia applicators, through-the-wall imaging equipment, wireless power transfer (WPT) and short-range communication systems, frequently require the synthesis of complex near-field distributions to enhance the resulting performances.

Several approaches have been proposed in literature to realize the aforementioned systems [1]–[7]. Microwave hyperthermia applicators employing antenna arrays to maximize RF energy deposition in patients' tumor tissues were proposed in [1]–[2]. WPT systems based on RF-focusing antenna arrays were developed in [3]–[5], while array systems and suitable detection algorithms for through-the-wall imaging were presented in [6]–[7].

Microwave and quasi-optical diffraction-resistant wave fields were proposed for short-range communications, micromanipulations and RF-focusing [8]–[10]. In [11], optical and millimeter wave high throughput short-range communication systems featuring Bessel beams carrying orbital angular momentum (OAM) to limit beam degradation by obstacles were presented. The optics-based system employs reflective spatial light modulators, while the RF one uses a spiral phase plate to yield an OAM beam from a Gaussian beam, and a metamaterial-based axicon to finally obtain the corresponding order OAM Bessel beam. The spiral plate establishing the required azimuthal phase shift can only be effective at quasi-optical wavelengths.

The generation of high-power Bessel and OAM Bessel beams using lasers was proposed in [12]. This approach yields non-diffractive beams and may be useful for long-range optical links due to their resilience against atmospheric perturbations affecting the field propagation. Finally, in [13], OAM Bessel beams were employed to realize a reflectarray generating cone-shaped radiation patterns in the Ka-band for mobile satellite communications.

In [14], two techniques were proposed to synthesize Airy beams propagating in opposite directions so as to focus electromagnetic energy in the Fresnel region of an array formed by uncoupled, infinitely long thin-wire antennas. The first one employs a linear array, featuring wire current magnitudes and phases given by the sampled Airy wave function over the aperture. The second one requires in-phase feeding of

The associate editor coordinating the review of this manuscript and approving it for publication was Shagufta Henna.

a thin-wire curved array arranged along a $3/2-$power-law surface profile to yield so-called "accelerating beams", showing that oppositely traveling Airy beams yield abruptly-autofocusing beam waves.

The aforementioned solutions, although fulfilling their intended application requirements, all feature static, non-reconfigurable radiative characteristics (e.g., antenna beam and near field angular scan) unless mechanical alterations are dynamically effected. Reconfigurable characteristics (either deterministic or adaptive) would however be desirable, for instance to improve detection accuracy of moving objects, perform selective scans over specific spatial regions inside objects or human subjects, and to sense or communicate beyond propagation obstacles (e.g., pillars and furnishings inside buildings, etc.).

Multiport radiating structures, intrinsically characterized by many degrees of freedom (i.e. radiating elements, their spatial arrangement and excitation profiles) may fulfill the aforementioned requirements if they are suitable to synthesize desirable field distributions in the near or far field region. To this end, this paper addresses the challenge of effecting near field synthesis and steering of complex field distributions (e.g., Bessel and Airy beams) by means of a rather basic square, planar dipole array, employing a novel field synthesis technique recently introduced in literature [15]. This technique exploits newly found, generalized orthogonality properties of the radiation matrix eigenfields, rigorously taking into account couplings among arbitrarily shaped and situated radiating elements, and was shown to provide very good accuracy in spot focusing RF energy and in synthesizing complex near-field distributions on target areas.

In this paper, the aforementioned field synthesis technique is extended to operate on open and closed synthesis surfaces, then used to synthesize target fields expressed in terms of either both $E-$ and $H-$fields or only the $E-$field. Besides comparing their respective synthesis performances, the robustness of the aforementioned techniques is investigated by carrying out a comprehensive sensitivity analysis with respect to random magnitude and phase variations of the array excitation profile, thus quantifying the impact of realistic non-ideal behaviors of the array feeding circuitry. Moreover, the technique is tested on the yet more challenging synthesis of tilted, untilted, and OAM Bessel beams, as well as on Airy beams, characterizing the spatial behavior of such diffraction-resistant field distributions when synthesized by means of a finite-size planar array. Numerical results yield quantitative performance metrics as well as design guidelines for choosing the better performing synthesis approach for the array excitation profile.

The paper is organized in four sections. In Section II, the field synthesis techniques for open and closed surfaces are illustrated. In Section III, the respective performances, including the degradation by random amplitude variations introduced by realistic array feeding circuitry, are compared. In the same Section, synthesis of tilted, untilted, and OAM Bessel beams, as well as Airy beams, are presented and their main propagation characteristics are discussed. Finally, concluding remarks are provided in Section IV.

II. FIELD SYNTHESIS TECHNIQUES

The circuital behavior of multi-port structures (circuits and antennas) can be fully described by the scattering matrix $\underline{\boldsymbol{S}}$, while their energetic behavior can be effectively and advantageously described through a set of Hermitian tensors: radiation matrix $\underline{\boldsymbol{Q}}_{rad}$, loss matrix $\underline{\boldsymbol{Q}}_{loss}$, and reactive power matrix $\underline{\boldsymbol{Q}}_{I}$ as illustrated in [15]. In particular, $\underline{\boldsymbol{Q}}_{rad}$ yields a multi-port antenna active power flow through an arbitrary (open or closed surface) S as

$$P_{rad} = \frac{1}{2}\,\mathrm{Re}\left\{\int_{S\left(\substack{\text{open}\\\text{closed}}\right)} \left[\boldsymbol{E}(\boldsymbol{r}) \times \boldsymbol{H}^{+}(\boldsymbol{r})\right]\cdot\hat{\boldsymbol{n}}\,dS\right\} = \frac{1}{2}\,\boldsymbol{a}^{+}\cdot\underline{\boldsymbol{Q}}_{rad}\cdot\boldsymbol{a} \tag{1}$$

where $\mathrm{Re}\{\cdot\}$ is the real part operator, "+" stands for the Hermitian transpose operator, $\hat{\boldsymbol{n}}$ is the normal unit-vector pointing outward (closed) or away from (open) the surface S, while $\boldsymbol{a}$ is the incident-wave excitation vector at its ports (see Fig. 1). The Poynting theorem states that P_{rad} is the total active power radiated by the multi-port structure when S encloses the antenna ($S = S_{closed}$).

The Hermitian character of the radiation matrix $\underline{\boldsymbol{Q}}_{rad}$ implies the following spectral decomposition

$$\underline{\boldsymbol{Q}}_{rad} = \sum_{i=1}^{N} \lambda_{rad_i}\,\hat{\boldsymbol{v}}_{rad_i}\,\hat{\boldsymbol{v}}_{rad_i}^{+} \tag{2}$$

where λ_{rad_i} and $\hat{\boldsymbol{v}}_{rad_i}$ are the eigenvalues and orthonormal eigenvectors of $\underline{\boldsymbol{Q}}_{rad}$, whose related eigenfields $\boldsymbol{e}_{R_i}(\boldsymbol{r})$ and $\boldsymbol{h}_{R_i}(\boldsymbol{r})$, excited when $\boldsymbol{a} = \hat{\boldsymbol{v}}_{rad_i}$ ($i = 1, 2, ...N$), fulfill the following, noteworthy generalized orthogonality integral relationship [15]

$$\frac{1}{2}\int_{S\left(\substack{\text{open}\\\text{closed}}\right)} \left[\boldsymbol{e}_{R_j}(\boldsymbol{r}) \times \boldsymbol{h}_{R_i}^{+}(\boldsymbol{r}) + \boldsymbol{e}_{R_i}^{+}(\boldsymbol{r}) \times \boldsymbol{h}_{R_j}(\boldsymbol{r})\right]\cdot\hat{\boldsymbol{n}}\,dS = \lambda_{rad_i}\delta_{ij}, \tag{3}$$

δ_{ij} being the Kronecker delta. The eigenvalues λ_{rad_i} express the realized radiation efficiencies (accounting for ohmic, dielectric, coupling, and mismatch losses) of the multiport antenna when $\boldsymbol{a} = \hat{\boldsymbol{v}}_{rad_i}$ and $S = S_{closed}$ encloses the array. The generalized orthogonality condition (3) can be exploited to synthesize target fields on closed or open surfaces as shown in [15], where two field synthesis techniques, denoted as "field-based", were introduced. The first one yields an optimal synthesis when both the target electric and magnetic field distributions are assigned on a given surface, while the second one requires only one of the fields to be assigned,

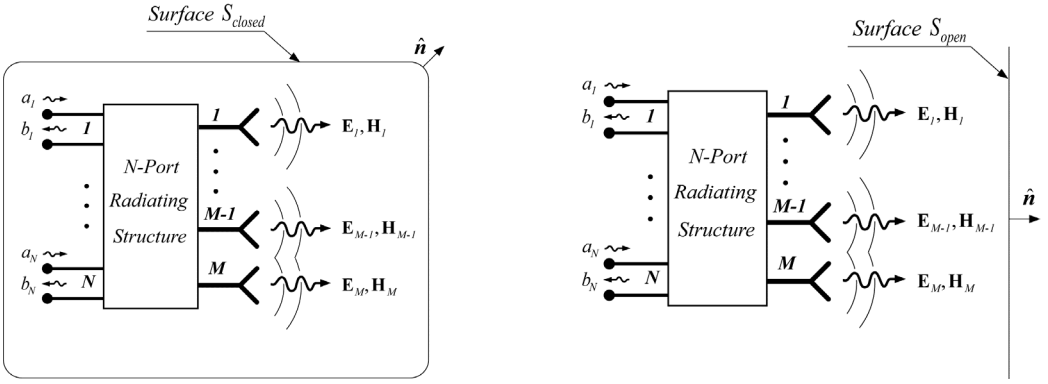

FIGURE 1. Schematic of the N-port radiating structure. The surfaces, (a) closed, and (b) open, on which the field synthesis is performed are shown in the figure.

thus providing a suboptimal synthesis. The optimal array excitation profile is derived as

$$\boldsymbol{a} = \frac{1}{2}\,\underline{\boldsymbol{V}} \cdot \underline{\boldsymbol{\Lambda}}^{-1} \cdot \boldsymbol{V}_{EH}, \tag{4}$$

where $\underline{\boldsymbol{V}} = \left[\hat{\boldsymbol{v}}_{rad_1}, \cdots, \hat{\boldsymbol{v}}_{rad_N}\right]$, $\underline{\boldsymbol{\Lambda}} = diag\left(\lambda_{rad_1}, \cdots, \lambda_{rad_N}\right)$ and $\boldsymbol{V}_{EH}$ is a vector whose components are given by

$$V_{EH_i} = \int\limits_{S\left(\substack{open\\closed}\right)} \left[\boldsymbol{E}(\boldsymbol{r}) \times \boldsymbol{h}_{R_i}^{+}(\boldsymbol{r}) + \boldsymbol{e}_{R_i}^{+}(\boldsymbol{r}) \times \boldsymbol{H}(\boldsymbol{r})\right] \cdot \hat{\boldsymbol{n}}\, dS, \tag{5}$$

$\boldsymbol{E}(\boldsymbol{r})$ and $\boldsymbol{H}(\boldsymbol{r})$ being the aforementioned target fields.

The suboptimal solution, when only the electric field is assigned, is instead given by

$$\boldsymbol{a} = \underline{\boldsymbol{V}} \cdot \left[2\,\underline{\boldsymbol{\Lambda}} - \underline{\boldsymbol{Z}}\right]^{-1} \cdot \boldsymbol{V}_E, \tag{6}$$

with

$$V_{E_i} = \int\limits_{S\left(\substack{open\\closed}\right)} \left[\boldsymbol{E}(\boldsymbol{r}) \times \boldsymbol{h}_{R_i}^{+}(\boldsymbol{r})\right] \cdot \hat{\boldsymbol{n}}\, dS, \tag{7}$$

$$Z_{ij} = \int\limits_{S\left(\substack{open\\closed}\right)} \left[\boldsymbol{e}_{R_i}^{+}(\boldsymbol{r}) \times \boldsymbol{h}_{R_j}(\boldsymbol{r})\right] \cdot \hat{\boldsymbol{n}}\, dS. \tag{8}$$

The optimal synthesis is numerically advantageous as it does not require any matrix inversion since $\underline{\boldsymbol{\Lambda}}$ is diagonal. However, as shown in the next Section in the case of field synthesis on open surfaces, significant numerical accuracy degradation in the field synthesis may occur if eigenfields featuring vanishingly small eigenvalues λ_{rad_i} are employed in Eq. (4), thus it is advisable omitting those eigenfields altogether by introducing a suitable cutoff threshold.

III. NUMERICAL RESULTS

The results presented in this section illustrate features and performances of the proposed techniques in the near-field synthesis on predefined closed or open surfaces, using both target electric and magnetic fields or just the former, as well as in near-field beam synthesis and steering. Target fields consisting of Bessel and Airy beams, characterized by limited diffractive effects [10], [14], and [16]–[18], were chosen due to their applicative relevance, making them suitable for applications in hyperthermia, surface inspections, secure short-range point-to-point communication, particles manipulation, nanosurgery, etc..

The proposed analysis addresses the near-field synthesis accuracy, as well as its sensitivity with respect to the excitation array profile, for a square dipole array using the normalized mean square error ($NMSE$) metric defined in [15] and reported below for the readers' convenience

$$NMSE_{\left(\substack{open\\closed}\right)}\Big|_{dB} = 10\,Log\frac{\displaystyle\int\limits_{S\left(\substack{open\\closed}\right)} \left|\boldsymbol{E}_t^{(Target)} - \boldsymbol{E}_t^{(\mathrm{Synthesized})}\right|^2 dS}{\displaystyle\int\limits_{S\left(\substack{open\\closed}\right)} \left|\boldsymbol{E}_t^{(Target)}\right|^2 dS} \tag{9}$$

to quantify the synthesis accuracy. Irrespective of whether the surface chosen for the field synthesis was open or closed, the parameter $NMSE$ was computed on both an open and a closed surface, so the subscripts "open" and "closed" for $NMSE$ were applied accordingly.

The multi-port array antenna employed in [15], featuring 21×21 $z-$oriented half-wave dipoles (length $145.4\,mm$, radius $1\,mm$) placed a $\lambda_0/4$ away from a $13.6\,\lambda_0 \times 13.6\,\lambda_0$ planar reflector, λ_0 being free-space wavenumber, and excited at $1\,GHz$ by $50\,\Omega$ sources, was adopted in the analysis

TABLE 1. Performance metrics for Bessel beams synthesis on closed surfaces for target areas located at several distances from the array.

E-H-Field Synthesis (*Unfiltered*)					
x_s	$NMSE_{open}$	$\eta_{rad_{open}}$	$NMSE_{closed}$	$\eta_{rad_{closed}}$	P_{in}
λ_0	-22.9 dB	81.9%	-22.6 dB	81.9%	0.965 mW
$2\lambda_0$	-20.0 dB	86.7%	-19.4 dB	86.8%	0.905 mW
$6\lambda_0$	-12.1 dB	83.2%	-11.2 dB	83.9%	0.881 mW
$10\lambda_0$	-8.1 dB	82.0%	-7.3 dB	83.3%	0.791 mW
E-H-Field Synthesis (*Filtered with threshold* $10^{-3}\lambda_{\max}$)					
λ_0	-23.1 dB	86.3 %	-22.8 dB	86.4 %	0.915 mW
$2\lambda_0$	-20.0 dB	87.2 %	-19.4 dB	87.3%	0.899 mW
$6\lambda_0$	-12.1 dB	85.8 %	-11.2 dB	86.5 %	0.855 mW
$10\lambda_0$	-8.1 dB	85.0 %	-7.3 dB	86.4%	0.763 mW

that follows. The dipoles are arranged on a square lattice featuring 180 *mm* (0.6 λ_0) distance between the center-fed dipole ports (5 *mm*−long gap sources). Coupling among dipoles and reflector, as well as diffractive processes, were rigorously modeled by a commercial software based on a full-wave method-of-moments (MoM) (FEKO v. 5.4 by Altair Engineering).

A. FIELD SYNTHESIS ON OPEN AND CLOSED SURFACES

In all cases addressed in the following, the closed surfaces describe a parallelepiped enclosing the antenna with a square base parallel to the array plane, featuring varying heights which identify the field synthesis square surfaces situated at several distances in front of the array.

A preliminary analysis involves the eigenvalues spectra corresponding to open and closed synthesis surfaces (see Fig. 2), where the open surfaces are square faces located in front of the array (see Fig. 1). Energy conservation law requires that the eigenvalues for any closed synthesis surface be independent of its shape. Noteworthy, it was observed that the eigenvalues spectra for open synthesis surfaces situated very close to the array is substantially similar to the closed-surface eigenvalue spectrum, while an increasing number of vanishingly small eigenvalues occur as the distance of the open synthesis surface increases, indicating that a correspondingly growing number of eigenfields spread RF energy outside the open synthesis surface, due in part to the diffractive processes at the array truncation [20]. As anticipated in Section II and remarked in the following, such an analysis of the eigenvalues spectrum is important since, in the synthesis based on target $E-$ and $H-$fields applied on open surfaces, eigenfields featuring vanishingly small eigenvalues could at times produce array excitation profiles causing field synthesis degradation, thus a lower number of eigenfields can be reliably employed for open surface synthesis at increasing distance from the array, de facto reducing the degrees of freedom available in the synthesis itself. Therefore, in the following analysis, synthesis results obtained using all the eigenfields (labeled *unfiltered modal synthesis*) are compared against results derived upon neglecting eigenfields with eigenvalues smaller than $10^{-3}\lambda_{\max}$(labeled *filtered modal synthesis*), $\lambda_{\max}$ being the largest eigenvalue.

A first example involves the synthesis of the zeroth-order finite-support Bessel beam defined in Appendix A, featuring peak amplitude $1V/m$ and radial wavenumber $\beta_\rho = 0.3\,\beta_0$, β_0 being the free-space wavenumber.

In Fig. 3 and 4 the spatial behaviors of the $z-$component of the synthesized electric field at $x_s = \lambda_0$ and $x_s = 10\lambda_0$, both filtered and unfiltered, are reported. The corresponding *NMSE*, efficiency, and incident power figures, including those for the intermediate distances $x_s = 2\lambda_0$ and $x_s = 6\lambda_0$, are provided in Tables 1 and 2 for the synthesis on closed and open target surfaces, respectively. As already mentioned, these performance metrics were computed on both open and closed surfaces, regardless of whether a target surface was closed or open, to derive a complete picture of the synthesis quality, and investigate features, advantages and drawbacks of each approach. For instance, Figs. 3a and 3b show that synthesizing a Bessel beam close to the array roughly yields similar performances for both open and closed synthesis surfaces,

TABLE 2. Performance metrics for Bessel beams synthesis on open surfaces for target areas located at several distances from the array.

E-H-Field Synthesis (*Unfiltered*)					
x_s	$NMSE_{open}$	$\eta_{rad_{open}}$	$NMSE_{closed}$	$\eta_{rad_{closed}}$	P_{in}
λ_0	-19.8 dB	44.5%	-19.4 dB	44.5%	1.777 mW
$2\lambda_0$	-19.0 dB	1.4%	-13.1 dB	1.5%	54.58 mW
$6\lambda_0$	-15.4 dB	0.40%	21.1 dB	49.1%	0.1950 W
$10\lambda_0$	-14.2 dB	0.0000066%	66.7 dB	34.6%	11.658 kW
E-H-Field Synthesis (*Filtered with threshold* $10^{-3}\lambda_{\max}$)					
λ_0	-23.0 dB	86.3 %	-22.4 dB	86.3 %	0.916 mW
$2\lambda_0$	-20.0 dB	86.0%	-18.1 dB	86.5%	0.915 mW
$6\lambda_0$	-14.0 dB	46.1%	0.0 dB	81.2%	1.659 mW
$10\lambda_0$	-9.6 dB	36.1%	2.8 dB	80.6%	1.965 mW

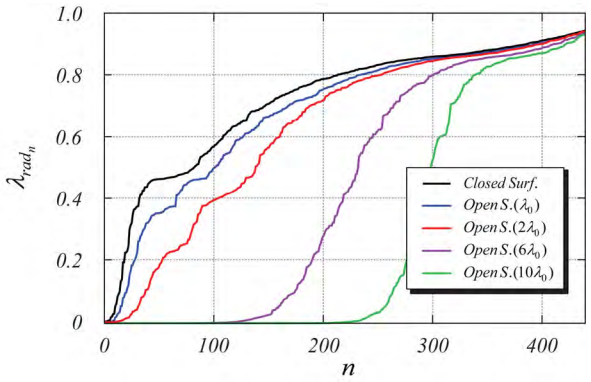

FIGURE 2. Eigenvalues spectrum of the radiation matrix as the distance from the synthesis surface varies. While for short distances from the synthesis surface the eigenvalues spectrum remains substantially similar to that of the closed surface, an increase in the number of vanishingly small eigenvalues can be observed as the distance of the open synthesis surface increases.

as confirmed in Tables 1 and 2 for $x_s = \lambda_0$ and $2\lambda_0$. Such a good agreement between the two techniques is due to the intrinsic limitation of the planar array in directing energy backwards and sideways towards low grazing angles. However, Figs. 3c and 3d show that at larger distances the power flowing through the lateral surfaces may grow significantly (open synthesis surface) unless the field is forced to vanish by a suitable choice of array excitation profiles (closed synthesis surface). This trend is confirmed by the performance data in Tables 1 and 2 ($x_s = 6\lambda_0$ and $10\lambda_0$), upon observing the large dB values attained by the *NMSE* when computed on the closed surface. On the other hand, open surface synthesis may provide better accuracy on the target area, as the smaller *NMSE* figures provided in the tables clearly indicate.

Lateral power flow may be undesirable due to emissions in unwanted directions and the increase in transmit power requirements for the RF electronics feeding the array. This is particularly relevant when the amplitude profiles are derived by synthesis on open surfaces, as shown in Tables 1 and 2 where the array input power P_{in}, defined as the total incident power at the ports, is also reported. For open surface synthesis there can be cases where the target field distribution is well approximated (low $NMSE_{open}$) even though the target-area efficiency is very low, as in the extreme case at $10\lambda_0$ featuring more than 11 kW incident power required, versus only about 0.8 mW needed for closed surface synthesis to obtain comparable error figures. The power flowing to the target area is indeed comparable in the two cases, as it can be readily verified multiplying efficiency and incident power, yet the choice of open surface synthesis has clear disadvantages, including strong undesirable emissions in unwanted directions, from a practical point of view. These drawbacks can be drastically cut down using modal filtering, upon removing from the synthesis process all eigenfields featuring eigenvalues lower than a specific threshold. Adopting an eigenvalue threshold of $10^{-3}\lambda_{\max}$ to limit the energetic impact was found to be effective in reducing lateral power flow for open synthesis surfaces, substantially preserving accuracy in the synthesis plane, as it can be seen comparing Figs. 3 and 4. As expected, modal filtering has a low impact on the lateral energy flow when the field synthesis is performed on closed surfaces. The spatial behavior of the main peak of

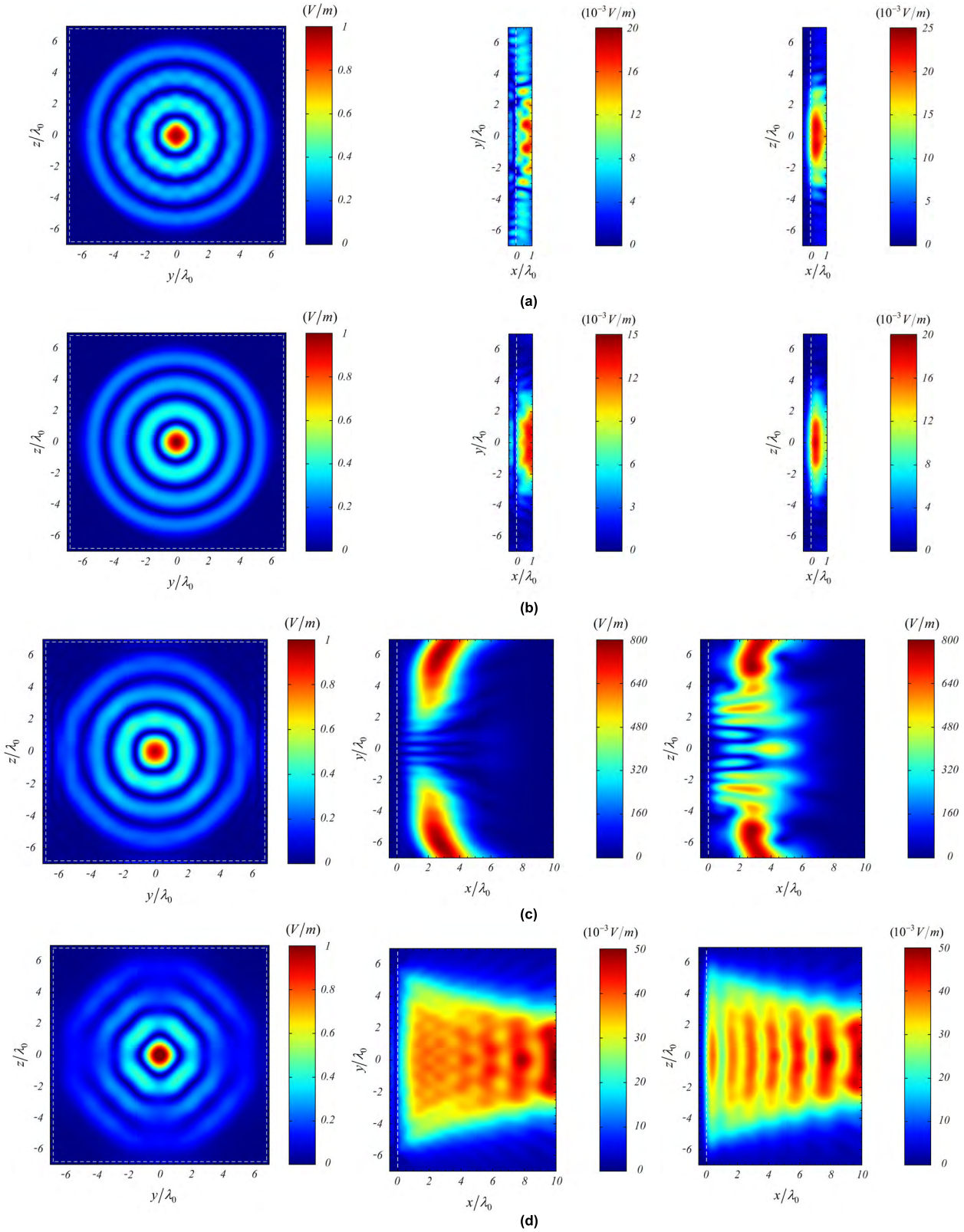

FIGURE 3. Spatial distribution of the electric field (z-component) of a Bessel beam synthesized without any modal filtering on an open surface at (a) $x_S = \lambda_0$, and (c) $x_S = 10\lambda_0$, and on a closed surface at (b) $x_S = \lambda_0$, and (d) $x_S = 10\lambda_0$. The field excited on the lateral surfaces surrounding the array are also shown. A white dashed line outlines the 21 × 21 element array reflector footprint.

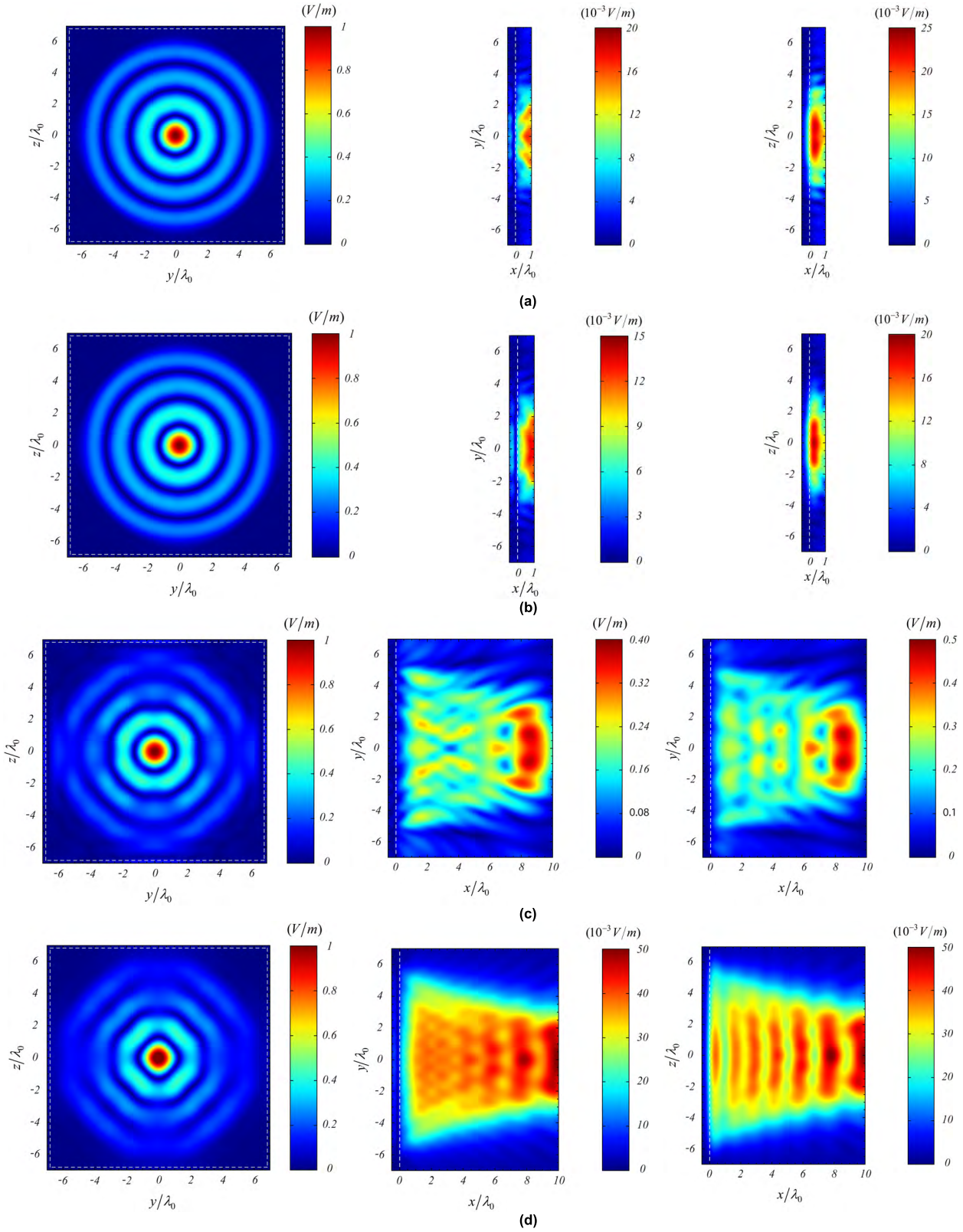

FIGURE 4. Spatial distribution of the electric field (z-component) of a Bessel beam synthesized by applying modal filtering on an open surface at (a) $x_S = \lambda_0$, and (c) $x_S = 10\lambda_0$, and on a closed surface at (b) $x_S = \lambda_0$, and (d) $x_S = 10\lambda_0$. The field excited on the lateral surfaces surrounding the array are also shown. A white dashed line outlines the 21 × 21 element array reflector footprint.